

ORIGINAL ARTICLE

Identification of rare heterozygous linkage R965C-R1309H mutations in the pore-forming region of SCN5A gene associated with complex arrhythmia

Yubi Lin^{1,2} | Jiading Qin¹  | Yuhui Shen^{1,3} | Jiana Huang⁴ | Zuoquan Zhang¹ | ZhiLing Zhu¹ | Huifang Lu¹ | Yin Huang¹ | Yuelan Yin¹ | Ani Wang¹ | Lizi Jin¹ | Zhenyu Hu¹ | Xiufang Lin¹ | Bin Jiang^{1,3}

¹The Cardiovascular Center, Department of Cardiology, Interventional Medical Center, Guangdong Provincial Key Laboratory of Biomedical Imaging and Guangdong Provincial Engineering Research Center of Molecular Imaging, The Fifth Affiliated Hospital, Sun Yat-sen University, Zhuhai, China

²Guangdong Provincial People's Hospital, Guangdong Academy of Medical Sciences, Guangdong Cardiovascular Institute, Guangzhou, China

³Guangdong Province Key Laboratory of Brain Function and Disease, Zhongshan School of Medicine, Sun Yat-sen University, Guangzhou, China

⁴Reproductive Medicine Center, The Sixth Affiliated Hospital of Sun Yat-Sen University, Guangzhou, China

Correspondence

Bin Jiang, Xiufang Lin, Zhenyu Hu, The Cardiovascular Center, Department of Cardiology, Interventional Medical Center, Guangdong Provincial Key Laboratory of Biomedical Imaging and Guangdong Provincial Engineering Research Center of Molecular Imaging, The Fifth Affiliated Hospital, Sun Yat-sen University, Zhuhai, 519000, China. Emails: jiangb3@mail.sysu.edu.cn; linxiufang_126@126.com; huzypku@hotmail.com

Funding information

Science and Technology Project of Zhuhai, Grant/Award Number: 20191210E030072; Medical Science and Technology Research Project of Guangdong Province, Grant/Award Number: A2018043; Natural Grant from National Natural Science Foundation of China, Grant/Award Number: 81970332; Natural Grant from National Natural Science Foundation of China, Grant/

Abstract

Background: We examined the genetic background of a Chinese Han family in which some members presented with complex arrhythmias including sick sinus syndrome, progressive conduction block, atrial fibrillation, atrial standstill and Brugada syndrome. The possible underlying mechanism associated with the genetic mutation was explored.

Methods: Targeted capture sequencing was conducted in the probands in the coding and splicing regions of genes implicated in inherited arrhythmias. Stable cell lines overexpressing wild type (WT) or mutant *SCN5A* were generated in HEK293T cells. Whole-cell recording was performed to evaluate the functional changes in sodium channels.

Results: The rare heterozygous linkage mutations, *SCN5A* R965C and R1309H, were found in these patients with complex familial arrhythmias. Compared to WT, R965C or R1309H, the peak current of sodium channel was dramatically reduced in HEK293T cell with linkage R965C-R1309H mutation when testing potentials ranging from -45 to 15 mV. Notably, the maximum peak current of sodium channels with R1309H and linkage R965C-R1309H displayed significant decreases of 31.5% and

Abbreviations: AVB, atrioventricular block; BrS, brugada syndrome; EVS, exome variant server; HGMD, the human gene mutation database; INR, international normalised ratio; MAF, minimum allele frequency; NC, negative control group; OMIM, online Mendelian Inheritance in Man; SIFT, scale-Invariant Feature Transform; SNPs, single-nucleotide polymorphisms; SSS, sick sinus syndrome; WT, wild type.

Yubi Lin, Jiading Qin and Yuhui Shen contributed equally to this work.

Yubi Lin, Jiading Qin and Yuhui Shen co-first author.

This is an open access article under the terms of the Creative Commons Attribution-NonCommercial-NoDerivs License, which permits use and distribution in any medium, provided the original work is properly cited, the use is non-commercial and no modifications or adaptations are made.

© 2021 The Authors. *Molecular Genetics & Genomic Medicine* published by Wiley Periodicals LLC.

Award Number: 81870869; National Key R&D Program of China, Grant/Award Number: 2017YFA0104704; Science and Technology Program of Guangdong Province, Grant/Award Number: 2014B070705005

73.34%, respectively, compared to WT. Additionally, compared to R965C or R1309H alone, the linkage mutation R965C-R1309H demonstrated not only a more obvious depolarisation-shifted activation and hyperpolarisation-shifted inactivation, but also a more significant alteration in the time constant, $V_{1/2}$ and the slope factor of activation and inactivation.

Conclusions: The linkage mutation *SCN5A* R965C-R1309H led to a more dramatically reduced current density, as well as more significant depolarisation-shifted activation and hyperpolarisation-shifted inactivation in sodium channels than R965C or R1309H alone, which potentially explain this complex familial arrhythmia syndrome.

KEYWORDS

atrial fibrillation, hereditary arrhythmia, *SCN5A*, sodium channel

1 | INTRODUCTION

The *SCN5A* gene (a highly conserved 100 kb gene) is located on chromosome 3 and contains 28 exons encoding the pore-forming α -subunit of the cardiac voltage-gated sodium channel ($Na_v1.5$), which is responsible for the generation and rapid propagation of action potentials in the heart via a fast inward sodium current (I_{Na}) (Nakaya, 2014). $Na_v1.5$ includes six transmembrane segments (S1–S6), which form a channel pore that determines the selectivity and permeability of sodium channel. As reported in the Online Mendelian Inheritance in Man (OMIM) database, pathogenic mutations in *SCN5A* (OMIM accession number 600163) have been demonstrated to contribute to a wide range of inherited and malignant arrhythmia syndromes, such as type 3 long QT syndrome, Brugada syndrome (BrS), familial progressive cardiac conduction defect, sick sinus syndrome (SSS), atrial fibrillation, atrial flutter, atrial standstill, ventricular fibrillation, dilated cardiomyopathy, arrhythmogenic cardiomyopathy, and sudden infant death syndrome.

Here, we reported complex familial arrhythmias in a Han Chinese family that is characterised by SSS, familial progressive cardiac conduction defect, atrial fibrillation, atrial flutter, atrial standstill, and BrS syndrome. In addition, the genetic background and possible underlying pathogenic mechanism were also explored.

2 | MATERIALS AND METHODS

2.1 | Ethical compliance

This clinical investigation was approved by the Guangdong Medical Institutional Review Board and Medical Ethics Committees [No.GDREC2016001H(R1)]. Informed written consent was obtained for all patients. The diagnostic criteria

of BrS morphology and SSS are shown in Supplemental methods.

2.2 | Genetic sequencing and bioinformatics analysis

The DNA from peripheral blood was conducted by the targeted capture sequencing, through the capture panel (NimbleGen). The panel contained 61 genes related to inherited arrhythmias (Supplemental methods). To predict the effect of missense variants, we used dbNSFP, which contained several well established in silico prediction programs (Scale-Invariant Feature Transform [SIFT] and PolyPhen-2). The pathogenic variants were assessed according to the protocol issued by ACMG (Richards et al., 2015). The Human Gene Mutation Database (HGMD) was used to screen mutations reported in published studies. DNA variants were considered disease-causing rather than polymorphisms if: (a) they were absent from the 1,000 Genomes exome database (<http://www.1000genomes.org>); (b) the minimum allele frequency (MAF) was <1% in the Exome Variant Server (EVS) of the NHLBI Exome Sequencing Project, which includes patients with cardiac diseases [<http://evs.gs.washington.edu/EVS/> (02-2013 accessed)]; and (c) they were present in highly conserved regions (<http://genome.cse.ucsc.edu/index.html>) (Wei et al., 2011). Gene mutations were annotated based on the sequence data in Genbank (Accession number NM_001099404 for *SCN5A*). The risk mutations were verified by Sanger sequencing among the families (Supplemental methods).

2.3 | Whole-cell recordings

Here, we use HEK293T cell strains to successfully construct stably transfected cells expressing WT, p.R965C, p.R1309H, and p.R965C-R1309H of *SCN5A* gene, respectively (Supplemental

methods). Whole-cell recordings were performed in HEK293T cells with a MultiClamp 700B amplifier controlled by pClamp 10.6. Experiments were performed at 31°C. To record the current density of sodium channel, patch pipettes (2–4 M Ω) made from borosilicate glass through the Sutter P-97 micropipette puller were filled with the internal solution containing the following elements (in mM): CsCl 50, CsF 30, L-aspartic acid 50, NaCl 10, tetraethylammonium hydroxide (TEA-OH) 11, EGTA 5, HEPES 10, pH 7.2–7.3 adjusted with CsOH, and with an osmolarity of 290–300 mOsm. The external solution for the sodium current recordings contained the following elements (in mM): NaCl 120, KCl 5.4, CaCl₂ 1.8, MgCl₂ 1, HEPES 10, glucose 10, tetraethylammonium chloride (TEA-Cl) 20, and with a pH of 7.2–7.4 adjusted with NaOH. Only cells with a series resistance less than 15 M Ω , compensated by 70%–90% (before compensation, WT: 11.46 \pm 0.83 M Ω , n = 81; R965C 12.30 \pm 1.05 M Ω , n = 40; R1309H: 11.16 \pm 1.18 M Ω , n = 29; and R965C-R1309H: 11.16 \pm 0.79 M Ω , n = 68, Kruskal–Wallis: 1.511; *p* = 0.68), and an input resistance greater than 600 M Ω were studied. On average, the cells from WT, R965C, R1309H and R965C-R1309H mutations had similar input resistances (WT: 731.73 \pm 38.88 M Ω , n = 81; R965C: 722.5 \pm 65.02 M Ω , n = 40; R1309H: 698.97 \pm 61.52 M Ω , n = 29; and R965C-R1309H: 723.38 \pm 38.99 M Ω , n = 68, Kruskal–Wallis: 0.215; *p* = 0.975). Data were filtered at 3 kHz and digitised at 10 kHz.

To detect the activation characteristics of the sodium current, we used a single-pulse voltage stimulation method: the sodium current was induced by a 50-ms depolarisation stimulation, which ranged from –100 mV to +60 mV with increments of 5 mV at a holding potential of –120 mV. To detect the steady-state inactivation characteristics of the sodium current, a two-pulse protocol was performed: the first pulse with a duration of 500 ms from –140 to –40 mV at 5 mV increments, followed in succession by the second pulse fixed at –40 mV, and the sodium current induced by the second pulse was the targeted current. Both steady-state activation and inactivation curves were fitted with the Boltzmann function: $I/I_{\max} = (1 + \exp(-(V - V_{1/2})/k))^{-1}$ and $I/I_{\max} = (1 + \exp((V - V_{1/2})/k))$ respectively. I/I_{\max} is the induced current normalised to its maximum value. V is the test potential. $V_{1/2}$ is the test voltage at which the current amplitude was half-maximum, and k is the slope factor. The time constant τ for steady-state activation and inactivation was obtained from the Clampfit software.

2.4 | Statistical analysis

Data analysis was performed with GraphPad Prism 5. All the data are presented as the mean \pm SEM. For the comparisons, both the slope factor (k) and $V_{1/2}$ were calculated using one-way ANOVA followed by the homogeneity test for variance,

while the rest of the data were analysed using the unpaired two-sample Student's *t*-test. A *p* < 0.05 was considered to be statistically significant.

3 | RESULTS

3.1 | Presentation of clinical cases

The familial pedigree is shown in Figure 1. Proband III: 7 in the third generation came for a medical consultation at 20 years old (in the year 2015). He suffered from SSS and a high-degree atrioventricular block (AVB) with syncope and dizziness, determined from an electrocardiogram when he was 10 years old (in the year 2005) (Figure 2a,b). Therefore, he was given a permanent cardiac pacemaker implant. Atrial fibrillation (Figure 2c) occurred 1 year after implantation and was recurrent even after catheter ablation at the age of 18. His father II:3 exhibited a complication of atrial flutter with fast ventricular rate (Figure 2d) at the age of 41 (in the year 2006), and was treated with catheter ablation. Because II:3 displayed SSS and intermittent third-degree AVB (Figure 2e) at the age of 46 (in the year 2011), he was ultimately given a permanent cardiac pacemaker. The ECGs of II:3 at the age of 50 (in the year 2015) (Figure 2f) showed regular ventricular pacing dependence with no discernible P waves and f waves, suggesting progressive and complete AVB and disappearance of atrial electrical activation. Furthermore, a peak representing left atrial contraction in the late diastolic period was absent in the echocardiogram. These phenomena indicated an atrial standstill. Three episodes of ischaemic cerebral stroke malignantly induced multiple softening cavities in bilateral cerebral hemispheres (Figure S2) likely due to persistent atrial fibrillation and atrial standstill (Figure 2f), which also consequently led to the disorder of limb activity, despite oral adequate anticoagulation using Warfarin (INR 2.0–3.0). The ECGs of II:2 showed type I (Figure 2g) and II BrS patterns. II:2 had a history of syncope associated with overexertion and lack of sleep without ECG recordings. III:3 had no malignant event but displayed apparent sinus bradycardia (mean heart rate \leq 40 bpm) in a daytime Holter recording (Figure 2h,i). III:4 and I:1 had an asymptomatic first-degree/intermittent second-degree and first-degree AVB, respectively, during 24-hour Holter recordings. The ECGs and 24-hour Holter recordings of other family members were normal. There were no significant abnormalities of cardiac structure in this family, as evaluated by echocardiography.

3.2 | Genetic backgrounds

After filtering single-nucleotide polymorphisms (SNPs) with MAF \geq 0.01, III:7 was identified to possess heterozygous

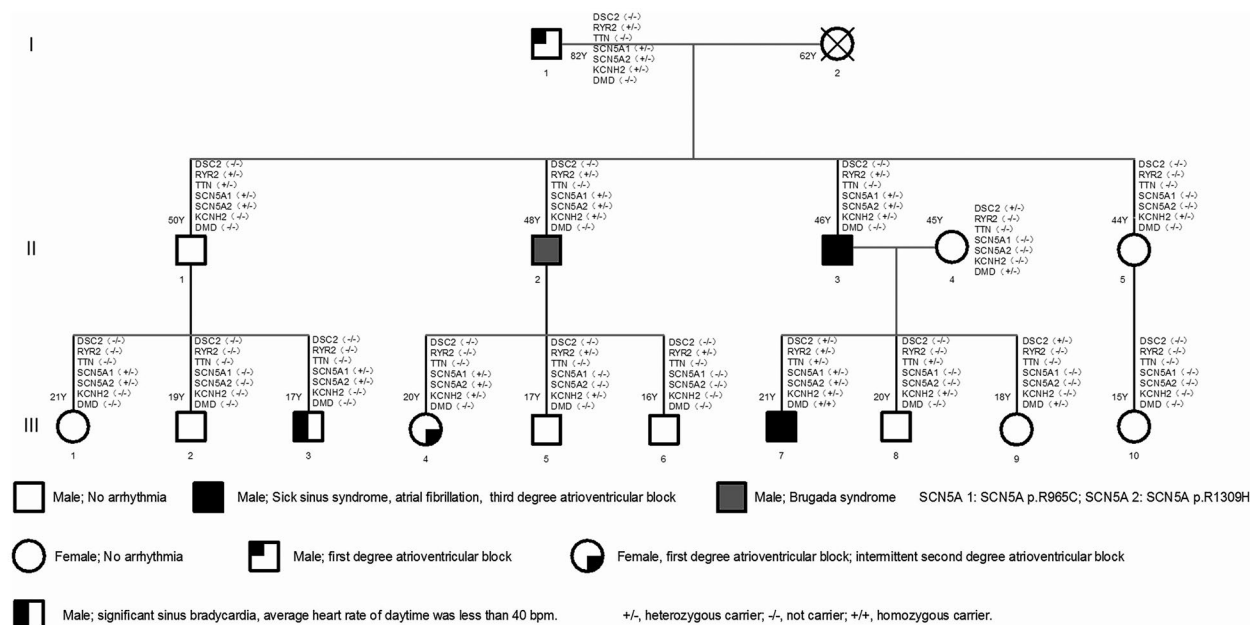


FIGURE 1 Familial pedigrees with *SCN5A* mutations. The gene abbreviations are as follows: *DSC2*, desmocollin 2; *RYR2*, ryanodine receptor 2; *TTN*, titin; *SCN5A*, sodium voltage-gated channel alpha subunit 5; *KCNH2*, potassium voltage-gated channel subfamily H member 2; *DMD*, dystrophin. ±, a heterozygous carrier with the mutation; —, no carrier with the mutation.

mutations in *SCN5A* (exon17:c.2893C>T, p.R965C), *SCN5A* (exon22:c.3926G>A, p.R1309H), *RYR2* (exon37: c.5614G>A, p.D1872N), *KCNH2* (exon9:c.3094C>T, p.R1032W), *DSC2* (exon15: c.C2497T, p.R833C), *TTN* (exon2: c.G13A, p.A5T) and *DMD* (exon9: c.G1140C, p.K380N), as shown in Table 1. The *RYR2*, *SCN5A* and *KCNH2* genes are associated with hereditary arrhythmia and cardiac ionic channelopathies, while the *DSC2*, *DMD* and *TTN* genes mostly lead to cardiomyopathies (Bezzina et al., 2015) (Jacoby & McKenna, 2012). Polymerase chain reaction-based sequencing of *SCN5A* (Figure 3a) showed a C-T transversion at codon 2893 of exon 17 and a G-A transversion at codon 3926 of exon 22, resulting in the substitution of arginine for cystine (R965C) and arginine for histidine (R1309H). The MAF of *SCN5A* R965C and R1309H was less than 0.001 in the Frequency of 1000 Genomes database. The risks of the pathogenesis of both mutations were predicted as ‘Damaging’ by the PolyPhen and SIFT algorithms. All these mutations mentioned above were validated by Sanger sequencing in all families, and the primers are shown in Table 2. The genotype–phenotype co-separation analysis (Figure 1 and Figure S3) revealed a heterozygous linkage pattern (R965C-R1309H), since the two heterozygous mutations of R965C and R1309H were passed down over generations, suggesting that the two mutations were located on the same chromosome. The members of this family, including I:1, II:1–3, III:1, III:3, III:4 and III:7, carried the heterozygous linkage R965C-R1309H. II:5, who carried the *KCNH2* mutation but not the *SCN5A* mutations, had normal ECGs and cardiac structure without arrhythmia at the age

of 44. III:3, carrying the heterozygous linkage *SCN5A* mutations but not the *KCNH2* and *RYR2* mutations, exhibited early sinus node dysfunction in the daytime. Furthermore, the *DSC2* and *DMD* mutations were also validated in II:4, who had no kinship to II:3. Besides, mutations in *TTN*, encoding the cardiac structure protein of titin, are common in the population. Moreover, there was no clinical evidence of cardiomyopathies in this family.

It is worth mentioning that II:3 and III:7 had similar clinical phenotypes characterised by SSS, atrial fibrillation and progressive disease of the cardiac conduction system. II:2 had BrS syndrome. III:3 had significant sinus bradycardia, suggesting early sinus node dysfunction, without causing clinical symptoms. It could be concluded that II:3, III:3 and III:7 had similar clinical phenotypes that might be related to myocardial channelopathies, while the disease-causing genotypes should be the same. The Sanger sequencing (Figure 1 and Figure S3) revealed that II:3, III:3 and III:7 all carried the heterozygous linkage *SCN5A* R965C-R1309H mutation. In particular, III:3 only carried the *SCN5A* R965C-R1309H mutation, and did not possess *DSC2*, *RYR2*, *TTN*, *KCNH2* or *DMD* mutations, indicating that the heterozygous linkage mutation *SCN5A* R965C-R1309H is the key factor for the onset of complex arrhythmia syndrome.

R965C located in the intracellular loop between domains II and III (DII-III) of the $Na_v1.5$ protein, and the $Na_v1.5$ was encoded by the *SCN5A* gene (Figure 3b). R1309H is located in the S4 helix of the transmembrane region of domain III (DIII) and functions as a voltage sensor in sodium channel. The conservation analyses demonstrated that R965 and R1309 were highly conserved across all species (Figure 3c).

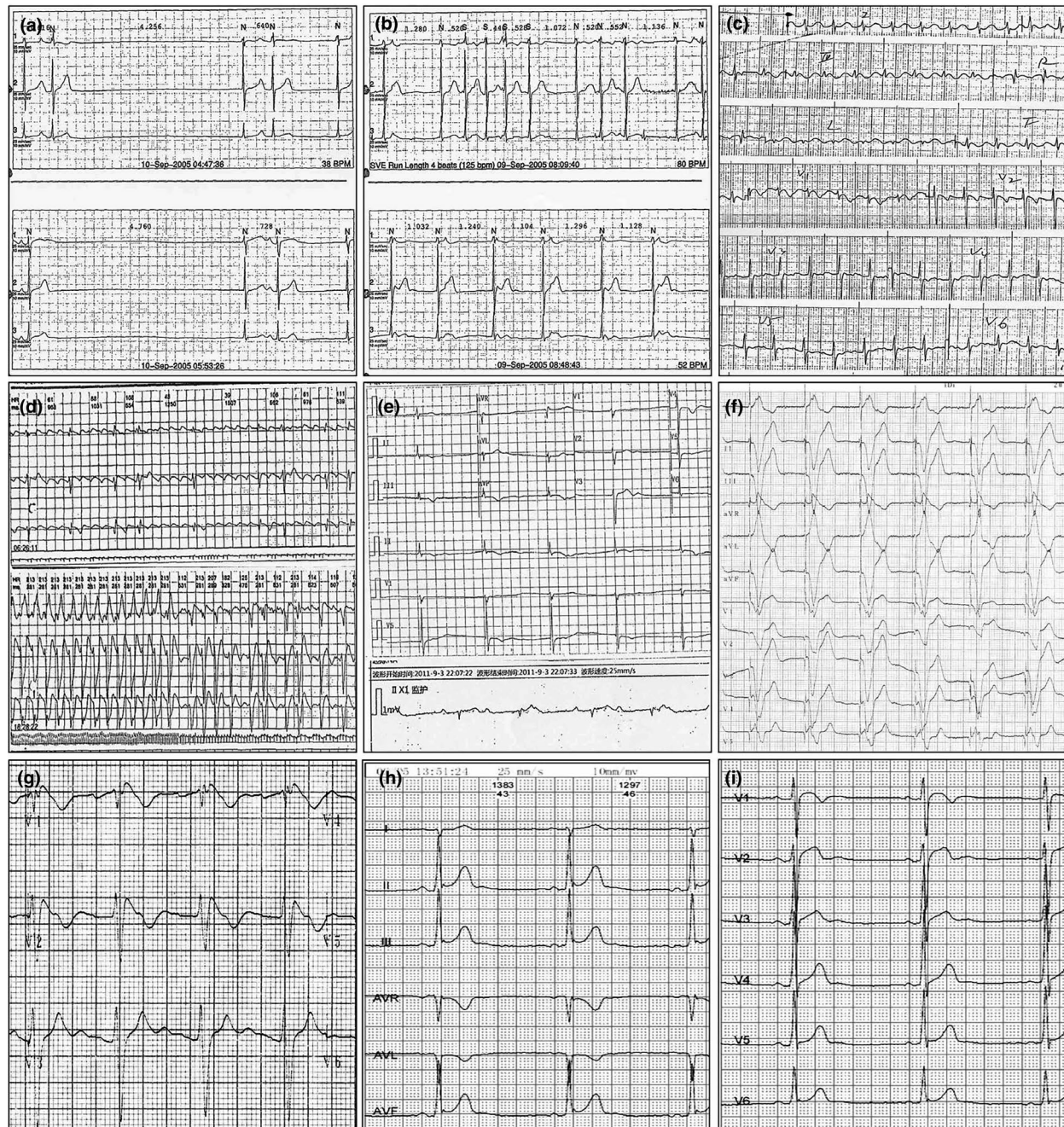


FIGURE 2 The electrocardiograms of family members with phenotypes. The ECGs of III:7 and II:3 are shown in (a-c and d-f) respectively. (a) Sinus arrest for approximately 4.25 (Top) and 4.76 (Bottom) seconds, junctional escape beat and premature atrial beat. (b) Top, sinus arrest, junctional escape beats, frequent premature atrial beats and short escapes of atrial tachycardia. Bottom, sinus arrest and junctional escape rhythm. (c) Atrial fibrillation with a fast ventricular rate. (d) Top, atrial flutter with 2:1 to 6:1 atrioventricular conduction. Bottom, atrial flutter with fast ventricular rate. (e) Top, sinus arrest and junctional escape rhythm. Bottom, third-degree atrioventricular block, and junctional escape rhythm. (f) Atrial standstill and persistent ventricular pacing, termed as ventricular pacing dependence. (g) ECG of II:2, Brugada-like ECG of type I. (h) ECG of III:3, apparent sinus bradycardia during the daytime.

3.3 | Electrophysiological characteristics

The stable cell strains overexpressed wild type (WT), p.R965C, p.R1309H and p.R965C-R1309H *SCN5A*, compared to the negative control (NC) group, which is shown in Figure S1c. It has been reported that the R1309H mutation,

but not the R965C mutation, significantly reduces the sodium current density (Hsueh et al., 2009) (Wang et al., 2016). To detect the effect of the linkage R965C-R1309H on the function of sodium channel, the overexpression lentivirus carrying WT, R965C, R1309H or R965C-R1309H *SCN5A* was stably transfected into HEK293T cells. In voltage-clamp

TABLE 1 The potential pathogenic mutations in target capture sequencing for III:7 patient.

Chr	Start	Ref	Alt	Gene	AAChange	1000g2015all	1000g2015eas	SIFT	PP	avsnp142
chr18	28648871	G	A	DSC2	NM_004949:exon15:c.C2497T:p.R833C	0.0020	0.0099	0.001D	0.992D	rs142410803
chr1	237778042	G	A	RYR2	NM_001035:exon37:c.G5614A:p.D1872N	—	—	0.045D	0.001B	—
chr2	179669357	C	T	TTN	NM_001256850:exon2:c.G13A:p.A5T	0.0002	0.0010	0.051T	0.999D	rs552620474
chr3	38603943	C	T	SCN5A	NM_198056:exon22:c.G3926A:p.R1309H	0.0002	—	0D	1D	rs537423012
chr3	38622757	G	A	SCN5A	NM_000335:exon17:c.C2893T:p.R965C	0.0002	0.0010	0D	0.999D	rs199473180
chr7	150644474	G	A	KCNH2	NM_172057:exon9:c.C2074T:p.R692W	0.0004	0.0020	0.18T	0.998D	rs373394254
chrX	32381067	C	G	DMD	NM_004011:exon9:c.G1140C:p.K380N	0.0011	0.0052	0.145T	0.917D	rs72468630

Note: For proband III:7, the mutations of 61 genes with minimum allele frequency (MAF) ≥ 0.01 were filtered. PP, predicted by PolyPhen-2; B, benign; D, damaging; T, tolerated; -, no-report; 1000G, 1000 genome project database (2015 version). The gene abbreviations were as follows: DSC2, desmocolin 2; RYR2, ryanodine receptor 2; TTN, titin; SCN5A, sodium voltage-gated channel alpha subunit 5; KCNH2, potassium voltage-gated channel subfamily H member 2; DMD, dystrophin.

configuration, R1309H, but not R965C, significantly reduced the sodium current density compared to the WT group at a series of test potentials ranging from -50 mV to -25 mV (Figure 4a-c and Table S1), which was consistent with the previous works (Hsueh et al., 2009) (Wang et al., 2016). However, the linkage mutation R965C-R1309H resulted in a much more severe reduction in sodium current density ranging from -55 to 20 mV compared to the WT group. Even compared to R1309H, the linkage R965C-R1309H still had a significantly lower sodium current density ranging from -55 to 15 mV. The peak current of the sodium channel with R1309H and R965C-R1309H was dramatically reduced by 31.5% (-127.54 ± 15.18 pA/pF, $p < 0.001$) and 73.34% (-49.66 ± 4.64 pA/pF, $p < 0.001$), respectively, while the peak current of sodium channel with R965C remains unchanged (-174.74 ± 17.66 pA/pF), compared to the WT group (-186.28 ± 11.10 pA/pF) (Figure 4c). Moreover, the R965C-R1309H mutation caused a significant shift in the steady-state activation of sodium channel (Table S2). R1309H caused a right-shift effect on the activation curve (Figure 5a), depolarised the $V_{1/2}$ and enlarged the slope factor (Table S3). The time constant of R1309H was amplified ranging from -55 to -40 mV when compared to the WT group, indicating that the sodium channel of R1309H was activated at the more depolarised membrane potential and took a prolonged time to run up to the peak current. In contrast to the WT group, R965C did not show significant changes in the above parameters. Compared to R1309H, R965C-R1309H induced a more substantial depolarised shift of the activation curve, $V_{1/2}$ and slope factor, suggesting that the R965C-R1309H sodium channel was activated at a much more depolarised membrane potential and displayed slower activation (Table S3). The activating time constant of the R965C-R1309H sodium channel was significantly extended compared to the WT group, between -50 and -40 mV (Figure 5b and Table S4), but the test potential was shortened to -55 and -50 mV compared to the R1309H sodium channel. We posited that this might be due to the small current of the R965C-R1309H sodium channel, which led to a decrease in time to reach the peak current.

Moreover, the R965C-R1309H mutation caused more intense damage in the steady-state inactivation of sodium channel (Figure 5c and Table S5). Both R965C and R1309H mutations showed the highest left-shift inactivation curve and hyperpolarised inactivation $V_{1/2}$, respectively (Table S3), suggesting a reduction in the availability of open channels. The inactivating time constants of R965C and R1309H mutations were significantly prolonged at the test potential between -140 and -80 mV, respectively, indicating that the peak amplitude took a longer time to decay (Figure 5d and Table S6). The slope factor of R1309H was significantly amplified, but that of R965C was not, compared to the WT group (Table S3). Notably, the inactivation

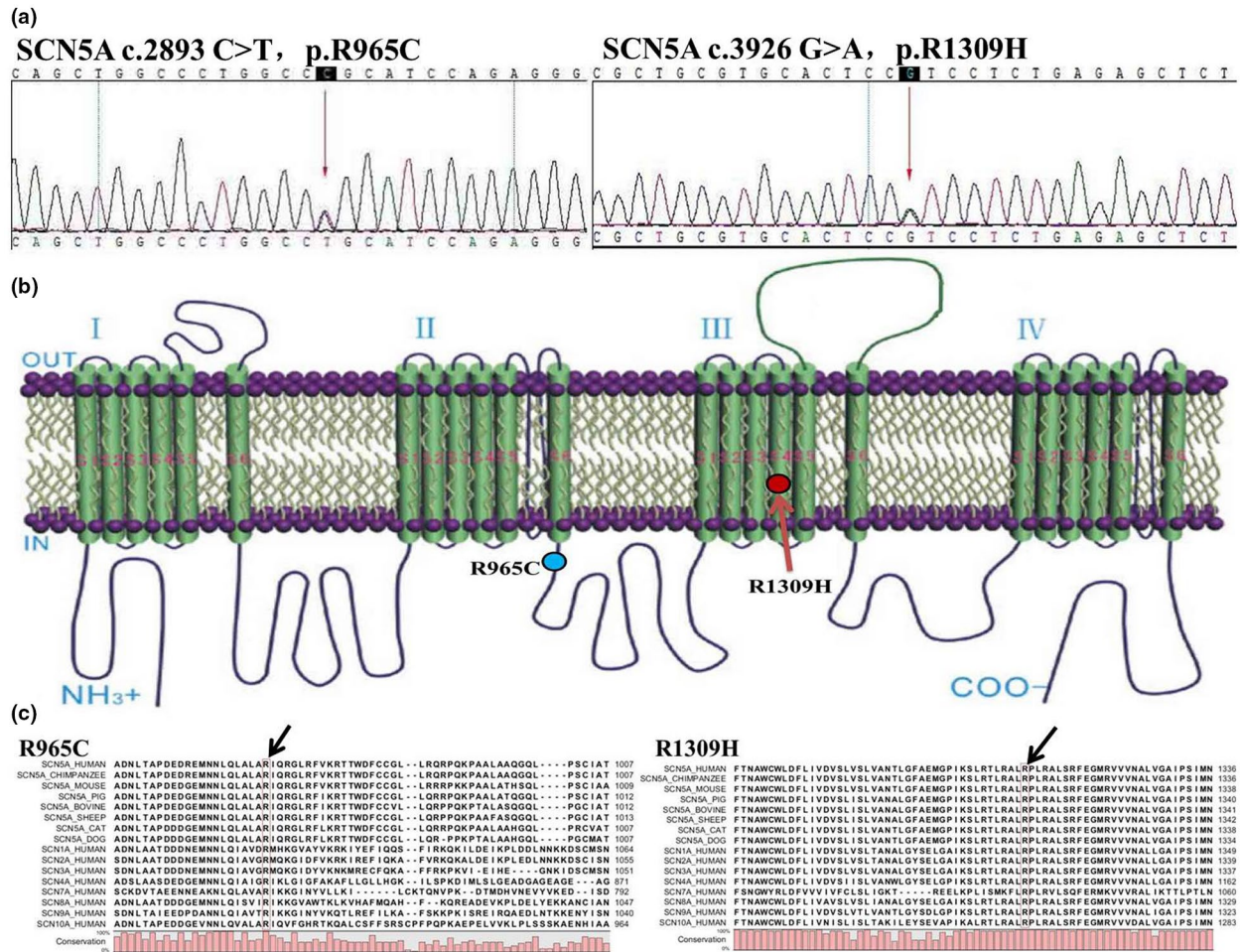


FIGURE 3 The molecular genetics of *SCN5A* linkage to complex familial arrhythmia syndrome. (a) Sanger sequencing of both the R965C and R1309H mutations. (b) R965C is located in the cytoplasmic loop between domains II and III. R1309H is located in the S4 helix of domain III as a voltage sensor. (c) The arginine at the 965 and 1309 sites of the amino acid sequence of Nav1.5 protein was conserved in all species.

TABLE 2 The primers of Sanger sequencing.

Gene	Location	Forward primer	Backward primer	Length
DSC2	chr18:28648871	5'GATCAGGAATCAAAAACGG3'	5'TAAAAAATAGGAGGGGAAGT3'	388
DMPK	chr19:46281745	5'GACCTGCTGACACTGCTGAG3'	5'AAAAGAGAAGGGTGGGATAAA3'	380
RYR2	chr1:237778042	5'GGAGAGTGACACGCTGGAGA3'	5'GAGTGAAATATGGGTGGAAAG3'	407
TTN	chr2:179669357	5'AAGCCACAAAAGAGAAGACC3'	5'AGCTGAGCCCAAATATAGAA3'	573
SCN5A	chr3:38603943	5'GTTCCCATCTCCCCATTTC3'	5'CTCGCCACAGTCTCCACG3'	282
SCN5A	chr3:38622757	5'CAGACAACCTCACAGCCCCT3'	5'CTGCCTTCTACCCCTACCCA3'	533
KCNH2	chr7:150644474	5'GAGCAGCGACACTTGCAAC3'	5'TCTCCCTTACCAGACAACACC3'	387
DMD	chrX:32381067	5'TGTATTTTCTGCATGTGCTT3'	5'CTTCTACCTTCCAGTCTTA3'	340

curve of R965C-R1309H was most significantly shifted to the left with the increase of $V_{1/2}$ hyperpolarisation and slope factor (Figure 5c and Table S3). Compared to the other two single mutations, the inactivation curve of R965C-R1309H was shifted further to the left, accompanied by further hyperpolarisation of $V_{1/2}$ and a further increase in slope factor, suggesting a much lower availability of open channels

(Figure 5c and Table S3). Although the inactivating time constant of R965C-R1309H was significantly longer than that of the WT group, it was in between the inactivating time constants of R1309H and R965C (Figure 5d and Table S6). Together, these results suggested that the linkage mutations, R965C and R1309H, demonstrated a synergistic effect on the pore-gating properties of sodium channel.

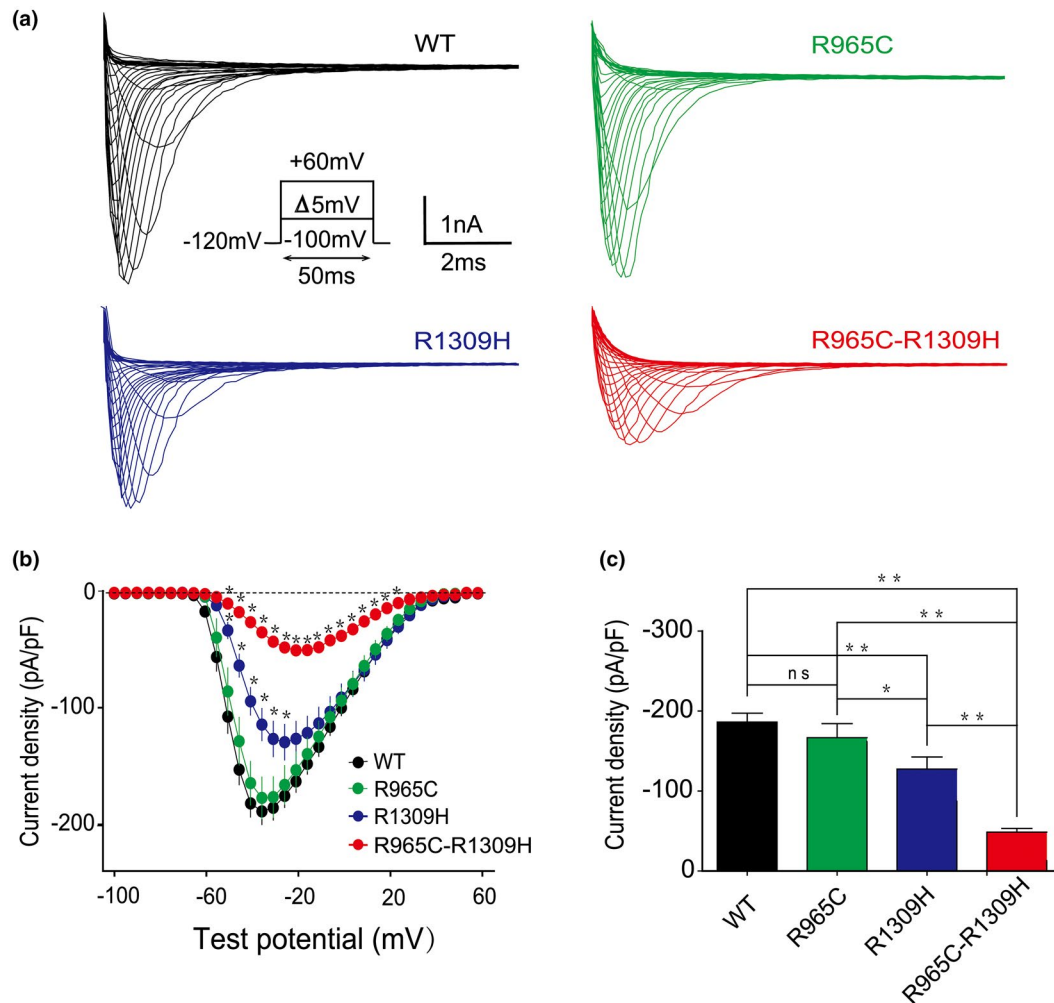


FIGURE 4 The peak currents of sodium channels recorded in HEK293 T cells. Voltage clamping on HEK293 T cells transfected with WT or mutant *SCN5A* at 31°C. (a) Representative traces of sodium channels with WT and mutant *SCN5A*. (b) The relationship of voltage (I-V) and current density of sodium channels with WT and mutant *SCN5A*. (c) The peak current of sodium channels with WT and mutant *SCN5A*. When compared to the WT group, a *p*-value of less than 0.05 was statistically significant. **p* < 0.05; ***p* < 0.01.

4 | DISCUSSION

In this study, we mainly discovered that the linkage mutations of R965C and R1309H exhibited a more significant reduction in current density, more depolarised activation and hyperpolarised inactivation of sodium channel in a synergistic way, which may be associated with complex familial arrhythmias and recurrent-serious cerebral embolisms.

According to previous studies (Hsueh et al., 2009) (Wang et al., 2016), the carrier with heterozygous R965C suffered from BrS, while the carriers with heterozygous R1309H showed slightly abnormal ECGs without arrhythmia events. Interestingly, we found in our study that the probands II:3 and III:7 carrying the heterozygous linkage mutation R965C-R1309H exhibited SSS, progressive AVB, atrial fibrillation and atrial standstill. The phenotypes of the heterozygous linkage mutation R965C-R1309H were different from those of heterozygous R965C or R1309H. As for the comparison

among the four groups with the function of sodium channel, the linkage R965C-R1309H led to the most malignant loss-of-function of sodium channel, including the lowest peak current density, slowest and depolarised activation, and most hyperpolarised inactivation of sodium channel, suggesting the largest reduction in the availability of open sodium channels. These changes induced by the linkage R965C-R1309H should decrease the action potential upstroke velocity and conduction velocity, thereby leading to cardiac conduction disease, including incomplete dysfunction or even complete loss of function of the sinus node, atrial propagation, atrio-ventricular node and intraventricular propagation.

The arginine at the 1309 site is located in the S4 helix of DIII of α subunit of $\text{Na}_v1.5$ protein. This S4 helix serves as a voltage sensor for sodium channel. The S4 in all four domains is involved in pore-gating to different extents. The S4 helices in DI-DIII seem to influence sodium channel activation, while the S4 of DIV seem to have a larger effect

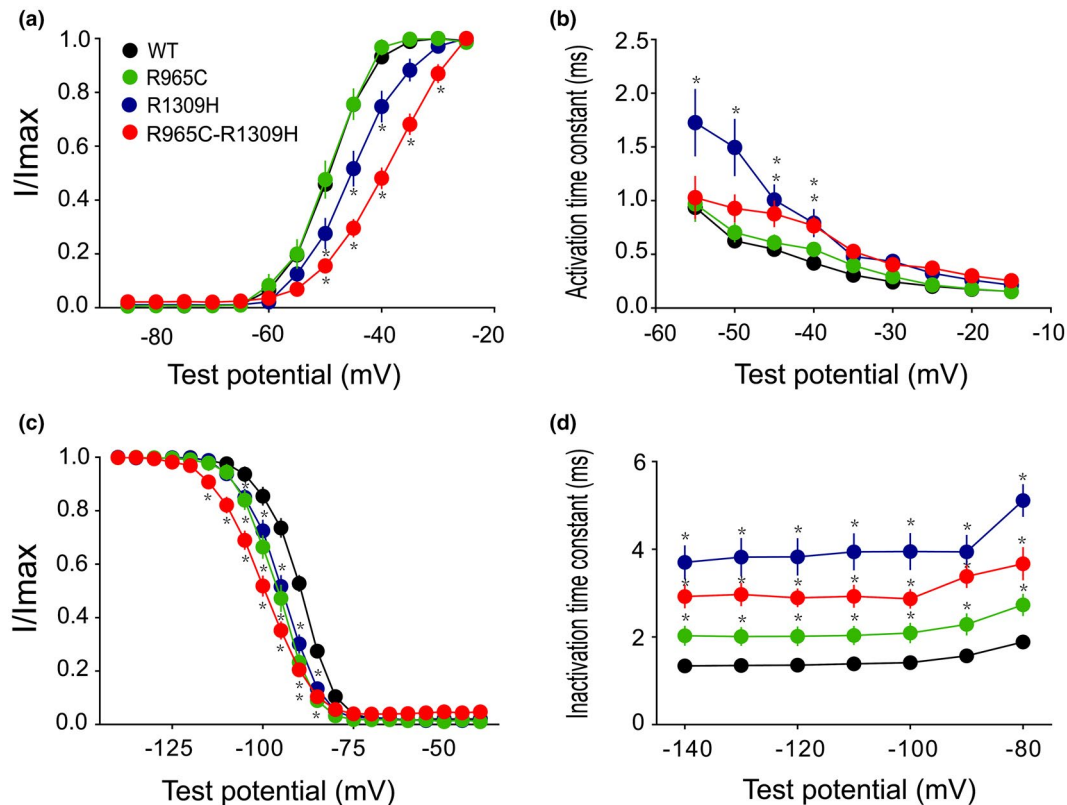


FIGURE 5 Kinetics of the sodium channel in steady-state activation and inactivation. (a) Steady-state activation as a function of voltage. (b) Relationship between tau (τ) and test potential for activation. (c) Steady-state inactivation as a function of voltage. (d) Relationship between tau (τ) and test potential for steady-state inactivation. When compared to the WT group, a p -value of less than 0.05 was statistically significant (*).

on inactivation than activation. The charged residues of S4 cause an outward motion of the helices towards the extracellular side of the membrane, which in turn induces conformational changes within the pore. The S4 helices also have molecular interactions with the surrounding S1–S3 helices, and thus facilitate activation (DeMarco & Clancy, 2016). We hypothesise that the spatial and conformational changes in the amino acid sequence of S4 induced by harmful *SCN5A* mutations, for example, R1309H, could lead to abnormal outward motion towards the extracellular side of the membrane, or abnormal molecular interaction. R965C located in the DII/DIII linker, resembling an S4 voltage sensor, is an important determinant of sodium pore-gating (Camacho et al., 2006). The linkage mutations of R965C and R1309H synergistically disrupted the pore-gating properties of sodium channel, suggesting the importance of the interaction between the S4-like region in the DII/DIII linker and the S4 helix of DIII.

Some *SCN5A* mutations, such as the heterozygous linkage R965C-R1309H in our study, and the D1275N and E1053K mutations reported in a previous study, might be associated with a malignant risk of recurrent embolism induced by atrial standstill, even though the CHA₂DS₂-VASc score was zero (Moreau et al., 2018). Whether higher levels of INR (oral

warfarin) or new oral anticoagulants should be recommended for atrial standstill associated with *SCN5A* mutations needs further clinical evaluation. In this family, the clinical phenotypes of carriers with the heterozygous linkage R965C-R1309H showed diverse and incomplete penetrance.

4.1 | Study limitations

There were several limitations in the present study. Our study contained only a family with eight patients who carried heterozygous linkage *SCN5A* R965C-R1309H mutation. Although whole-cell recording demonstrated that the function of sodium channel in HEK293T cells was severely affected by the heterozygous linkage *SCN5A* R965C-R1309H mutation, we could not completely exclude the possibility that patient phenotype may derive from the combination of multiple mutations on different genes and not the sole effect of the heterozygous linkage *SCN5A* R965C-R1309H mutation. The lack of extensive genetic evaluation in family members potentially underestimated the connection between the heterozygous linkage mutation and patient phenotype.

5 | CONCLUSION

In summary, the linkage mutation of *SCN5A* R965C-R1309H resulted in a reduction in current density, significant depolarisation-shifted activation and hyperpolarisation-shifted inactivation of the sodium current, suggesting that R1309H further aggravated the pore-gating changes of sodium channel caused by R965C. Therefore, patients presented with linkage mutation of *SCN5A* R965C-R1309H mutation seemed more likely to suffer from severe arrhythmia. Our study called for further research to better elucidate the pathological mechanism between *SCN5A* R965C and R1309H mutations.

ACKNOWLEDGEMENTS

We thank Shulin Wu, Chunyu Deng, Zhixin Shan, Fang Rao and Jiening Zhu from Guangdong Cardiovascular Institute, and YanYan from The Fifth Affiliated Hospital of Sun Yat-sen University, for clinical and experimental assistance as well as genetic counselling. We are grateful to Jinsheng Tao (BGI, Shenzhen, China) for technical assistance. We also thank P. Suzanne Hart for help in revising the article.

The study was supported by the Science and Technology Project of Zhuhai (20191210E030072) to YBL, the Medical Science and Technology Research Project of Guangdong Province (A2018043) to YBL, the Natural Grant from National Natural Science Foundation of China (81870869 to BJ and 81970332 to ZYH), the National Key R&D Program of China (2017YFA0104704) to BJ and the Science and Technology Program of Guangdong Province (2014B070705005) to SLW.

CONFLICT OF INTEREST

The authors declare no conflict of interest.

ETHICAL APPROVAL

This study was approved by the Guangdong Medical Institutional Review Board and Medical Ethics Committees.

INFORMED CONSENT

Informed consent was obtained from all participants for whom identifying information is included in this article.

ORCID

Jiading Qin  <https://orcid.org/0000-0003-1688-3808>

REFERENCES

- Bezzina, C. R., Lahrouchi, N., & Priori, S. G. (2015). Genetics of sudden cardiac death. *Circulation Research*, *116*, 1919–1936.
- Camacho, J. A., Hensellek, S., Rougier, J. S., Blechschmidt, S., Abriel, H., Benndorf, K., & Zimmer, T. (2006). Modulation of Nav1.5 channel function by an alternatively spliced sequence in the DII/DIII linker region. *Journal of Biological Chemistry*, *281*, 9498–9506.
- DeMarco, K. R., & Clancy, C. E. (2016). Cardiac Na channels: structure to function. *Current Topics in Membranes*, *78*, 287–311.
- Hsueh, C. H., Chen, W. P., Lin, J. L., Tsai, C. T., Liu, Y. B., Juang, J. M., Tsao, H. M., Su, M. J., & Lai, L. P. (2009). Distinct functional defect of three novel Brugada syndrome related cardiac sodium channel mutations. *Journal of Biomedical Science*, *16*, 23.
- Jacoby, D., & McKenna, W. J. (2012). Genetics of inherited cardiomyopathy. *European Heart Journal*, *33*, 296–304.
- Moreau, A., Janin, A., Millat, G., & Chevalier, P. (2018). Cardiac voltage-gated sodium channel mutations associated with left atrial dysfunction and stroke in children. *Europace*, *20*, 1692–1698.
- Nakaya, H. (2014). *SCN5A* mutations associated with overlap phenotype of long QT syndrome type 3 and Brugada syndrome. *Circulation Journal*, *78*, 1061–1062.
- Richards, S., Aziz, N., Bale, S., Bick, D., Das, S., Gastier-Foster, J., Grody, W. W., Hegde, M., Lyon, E., Spector, E., Voelkerding, K., & Rehm, H. L. (2015). Standards and guidelines for the interpretation of sequence variants: a joint consensus recommendation of the American College of Medical Genetics and Genomics and the Association for Molecular Pathology. *Genetics in Medicine*, *17*, 405–424.
- Wang, H. G., Zhu, W., Kanter, R. J., Silva, J. R., Honeywell, C., Gow, R. M., & Pitt, G. S. (2016). A novel NaV1.5 voltage sensor mutation associated with severe atrial and ventricular arrhythmias. *Journal of Molecular and Cellular Cardiology*, *92*, 52–62.
- Wei, X., Ju, X., Yi, X., Zhu, Q., Qu, N., Liu, T., Chen, Y., Jiang, H., Yang, G., Zhen, R., Lan, Z., Qi, M., Wang, J., Yang, Y. I., Chu, Y., Li, X., Guang, Y., & Huang, J. (2011). Identification of sequence variants in genetic disease-causing genes using targeted next-generation sequencing. *PLoS One*, *6*, e29500.

SUPPORTING INFORMATION

Additional Supporting Information may be found online in the Supporting Information section.

How to cite this article: Lin Y, Qin J, Shen Y, et al. Identification of rare heterozygous linkage R965C-R1309H mutations in the pore-forming region of *SCN5A* gene associated with complex arrhythmia. *Mol Genet Genomic Med*. 2021;9:e1613. <https://doi.org/10.1002/mgg3.1613>